

Tunable ferrimagnetic-antiferromagnetic response by the inclusion of Fe in the gadolinium-based manganite GdMnO_3

Respuesta ferrimagnética-antiferromagnética sintonizable mediante la inclusión de Fe en la manganita basada en gadolinio GdMnO_3

Jorge A. Cardona-Vasquez ^{1a}, David A. Landínez-Téllez ^{1b}, Jairo Roa-Rojas ^{1c}

¹ Grupo de Física de Nuevos Materiales, Departamento de Física, Universidad Nacional de Colombia, Colombia.

Orcid: ^a 0000-0001-5771-837X, ^b 0000-0001-7108-617X, ^c 0000-0002-5080-8492

Emails: ^a joacardonava@unal.edu.co, ^b dalandinezt@unal.edu.co, ^c jroar@unal.edu.co

Received: 12 December 2019. Accepted: 28 March 2020. Final version: 4 April 2020.

Abstract

In this work a study of the synthesis process, crystal structure and magnetic behavior of gadolinium manganite with Fe substitutions in Mn positions of $\text{GdMn}_{1-x}\text{Fe}_x\text{O}_3$ ($x=0, 0.1, 0.2$) is reported. The samples were synthesized by the conventional solid-state reaction method. Structural characterization of final compounds was analyzed by Rietveld refinement, which revealed its crystallization in an orthorhombic symmetry belonging to the Pbnm (No. 62) space group. Results reveal that a and c cell parameters and the unit cell volume increase, while the lattice parameter b and the cell volume decrease with Fe substitution. The main effect in the structure is related to oxygen positions, i.e. in the octahedral distortions and rotations. DC susceptibility measurements, in the temperature regime between 4 K and 300 K on the application of an external field of 200 Oe, show a paramagnetic feature at high temperatures for all x studied values, with magnetic transitions associated to a magnetic ordered state at low temperatures ($21.8 \text{ K} < T < 25.2 \text{ K}$). Meanwhile, a ferrimagnetic transition is detected for $x=0.1$ close to $T=30.7 \text{ K}$. In order to explain the appearance of ferrimagnetism for this configuration, a model is suggested where an imbalance in the magnetic structure of GdMnO_3 (type-A antiferromagnetic) generated due to the introducing a Fe^{3+} ion in each pair consecutive unit cells is proposed. The effective magnetic moment obtained agrees to the reported value for the material with $x=0.0$, confirming the ferrimagnetic behavior for this concentration of Fe^{3+} in the structure.

Keywords: crystalline structure; magnetic feature; rare-earth based perovskite; ferri- antiferromagnetic transition.

Resumen

En este trabajo es reportado el proceso de síntesis, la estructura cristalina y el comportamiento magnético de gadolinio manganita con sustituciones de Fe en las posiciones Mn del material $\text{GdMn}_{1-x}\text{Fe}_x\text{O}_3$ ($x = 0, 0.1, 0.2$). Las muestras fueron sintetizadas por medio del método convencional de reacción en estado sólido. La caracterización estructural de los compuestos finales se analizó mediante refinamiento de Rietveld, el cual reveló su cristalización en una simetría ortorrómbica perteneciente al grupo espacial Pbnm (No. 62). Los resultados revelan que los parámetros de red a y c y el volumen de la celda aumentan, mientras que el parámetro de la red b y el volumen de la celda disminuyen con la sustitución de Fe. El efecto principal en la estructura está relacionado con las posiciones de oxígeno, es decir, con las

distorsiones y rotaciones octaédricas. Las mediciones de susceptibilidad DC, en el régimen de temperatura entre 4 K y 300 K bajo la aplicación de un campo externo de 200 Oe, muestran una característica paramagnética a altas temperaturas para todos los valores estudiados de concentración x , con transiciones magnéticas asociadas a un estado magnético ordenado a bajas temperaturas ($21,8 \text{ K} < T < 25,2 \text{ K}$). Entretanto, se observa la ocurrencia de una transición ferrimagnética para $x = 0.1$ cerca de $T = 30.7 \text{ K}$. Para explicar la aparición de ferrimagnetismo en esta configuración, se sugiere un modelo en el cual se propone la generación de un desequilibrio en la estructura magnética de GdMnO_3 (antiferromagnético tipo A) debido a la introducción de un ion Fe^{3+} en cada par de celdas unitarias consecutivas. El momento magnético efectivo obtenido concuerda con el valor reportado para el material con $x = 0.0$, confirmando el comportamiento ferrimagnético para esta concentración de Fe^{3+} en la estructura.

Palabras clave: estructura cristalina; carácter magnético; perovskita basada en tierra rara; transición ferri-antiferromagnética.

1. Introduction

The perovskites are a group of ceramic materials in which metallic and non-metallic elements are combined [1]. There is a wide variety of behaviors and physical and chemical properties associated with perovskite type materials, which arise from the relative ease of choice of cations A and B that may occupy the structural sites within the general composition ABX_3 , where X it is usually oxygen (in perovskite oxides) [2]. Commonly, position A is occupied by alkaline, alkaline earth, or rare-earth ions, while site B is occupied by transition metals (and even rare-earths), resulting in a huge number of possible combinations associated with different microscopic mechanisms that give rise to the interesting and sometimes exotic properties that characterize the perovskites, turning them into an attractive group of materials in relation to the possibility of technological applications that derive from that properties [3].

Perovskite manganese-based oxides (manganites) are good examples of the types of compounds in this family that show properties of extreme interest in materials science [4]. Particularly, family of manganites which are based on rare-earth elements have been extensively studied in recent years, because their properties mainly associated with the interaction between the rare-earth- $4f$ orbitals and the Mn- $3d$ orbitals, which give rise to very interesting magnetic behaviors and electrical transport properties [5]. This kind of material are recognized because evidence properties as antiferromagnetism [6], ferroelectric response, spontaneous or induced by magnetic fields [7], magnetoelectricity [8], giant and colossal magnetoresistance [9], and exchange interactions involving the Mn^{3+} and R^{3+} (rare-earth) magnetic moments [10].

Although this set of varied and exotic physical properties evidenced by the manganites are very striking for possible applications in spintronics technology, the particular interest of this work has to do with the multiferroic properties that show the materials of type

RMnO_3 , where R represents a rare-earth cation [11]. The properties mentioned here depend on the study temperature range of the materials, as well as the rare-earth ion included in them. Studies on the effect of the partial substitution of iron at the crystallographic site A on the magnetic properties of the manganese AMnO_3 have been carried out for the specific case $\text{A}=\text{Y}$ [12]. Meanwhile, there are still physical properties that can be studied on the partial inclusion of Fe in the sites of Mn of the rare earth manganite RMnO_3 [13-15], therefore, the aim of this work is to report the production process of the rare-earth manganite type $\text{GdMn}_{1-x}\text{Fe}_x\text{O}_3$ ($x=0.0, 0.1$ and 0.2), as well as the results of the study of the effect of this substitution of Fe^{3+} in the Mn^{3+} site about its crystallographic and magnetic properties, in order to determine the changes that could suggest improvements in the multiferroic behavior of this material.

2. Experimental setup

Samples of the $\text{GdMn}_{1-x}\text{Fe}_x\text{O}_3$ system ($x=0.0, 0.1$ and 0.2) were solid-state reacted following the conventional ceramic method, following the procedure described by C.A. Triana et al [16]. The masses of the precursor Gd_2O_3 (Sigma-Aldrich 99.99%), Mn_2O_3 (Sigma-Aldrich 99%) and Fe_2O_3 (Sigma-Aldrich 99%) oxides required to produce samples of 1.2 g were determined in stoichiometric proportions. These were submitted to a dried process at $160 \text{ }^\circ\text{C}$ for 1 h, weighted, mixed and grounded in an agate mortar around 2 h.

Then, the resultant the powder mixture was subjected to thermal calcination treatments at $700, 800$ and $900 \text{ }^\circ\text{C}$. Subsequently, the materials were pressed into pellets under a pressure 10 ton/cm^2 , and subjected to sinterization treatments at $1000, 1100$ and $1200 \text{ }^\circ\text{C}$. In the intermediate between each heat treatment, the powder was ground and its structure was analyzed through X-ray diffraction (XRD) experiments, at room temperature by using a X'pert PRO PANalytical powder X-ray diffractometer equipment, with $\text{Cu-}k\alpha$ radiation ($\lambda=1.54056 \text{ \AA}$), in the 2θ regime from 20° and up to 70° ,

with 0.02° degree-step and 20 s time-step. Characterization of magnetic response was performed by means curves of DC susceptibility as a function of temperature, which were measured in a Magnetic Properties Measurement System (MPMS-Quantum Design), in temperature values between 4 K and 300 K, on $H=200$ Oe applied field.

3. Results and discussion

The evolution of the crystalline structure during the thermal treatments related to the synthesis process of the material $GdMn_{1-x}Fe_xO_3$ by means of the solid-state reaction technique was carried out by XRD experiments. Figure 1 exemplifies in detail the structural evolution of these materials after being subjected to different

temperatures within the corresponding thermal treatments.

When a comparison of the diffraction peaks for different values of x is made, small changes in the 2θ positions are perceived, but also changes in the intensity ratio as a result of the substitution of Fe^{3+} in the Mn^{3+} sites of the crystal structure of the materials are evidenced. The identification process of the symmetry and corresponding space group of the final samples was carried out through the PANalytical X'Pert HighScore Plus software, while the type Rietveld refinement of the experimental X-ray data was made by using the GSAS code with the graphical interface EXPGUI [17-18].

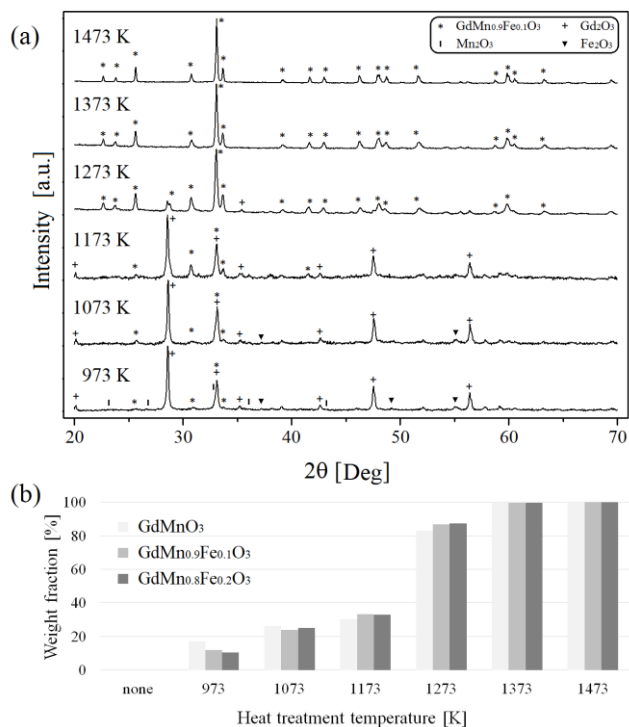


Figure 1. (a) XRD analysis of the structural evolution of the $GdMn_{0.9}Fe_{0.1}O_3$ compound during synthesis process.

Figure shows the 2θ peak positions corresponding to precursor oxides (Gd_2O_3 , Mn_2O_3 and Fe_2O_3) and the peak positions of $GdMn_{0.9}Fe_{0.1}O_3$. (b) Quantification of phase formation for the x concentrations in $GdMn_{1-x}Fe_xO_3$.

Source: Authors.

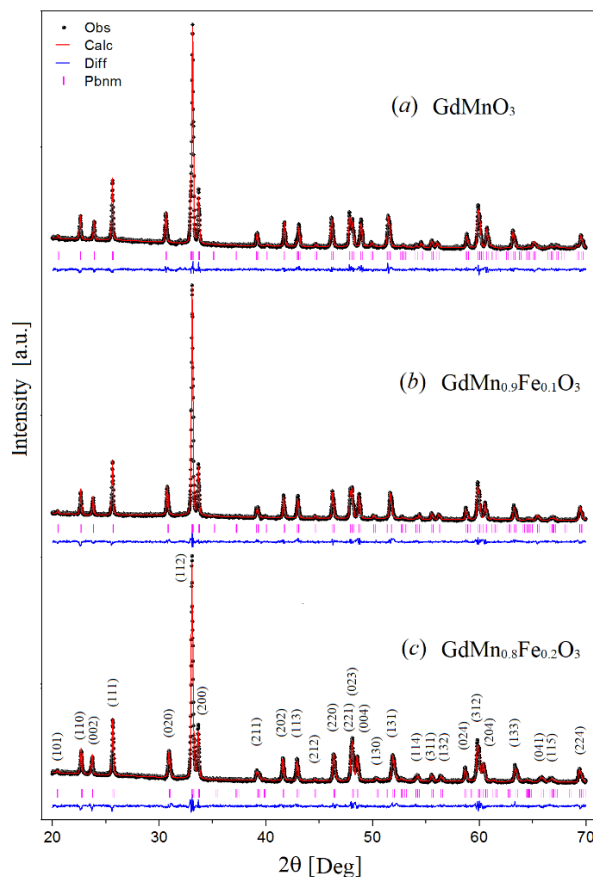


Figure 2. Refined patterns of the $GdMn_{1-x}Fe_xO_3$ compounds with $x=0.0$ (a), $x=0.1$ (b) and $x=0.2$ (c). In the picture, points represent the experimental data, red lines are the theoretical diffractograms, blue lines are the difference and the short magenta lines indicate the position of the peaks corresponding to the orthorhombic structure, Pbnm (#62) space group.

Source: Authors.

Table 1. Lattice parameter after the refinement procedure for $GdMn_{1-x}Fe_xO_3$ compounds

Compound			$GdMnO_3$	$GdMn_{0.9}Fe_{0.1}O_3$	$GdMn_{0.8}Fe_{0.2}O_3$
Cell Parameters					
a [Å]			5.3172(1)	5.3187(1)	5.3207(1)
b [Å]			5.8334(1)	5.8072(1)	5.7769(2)
c [Å]			7.4431(2)	7.4688(2)	7.4952(2)
Cell Vol [Å ³]			230.87(1)	230.67(1)	230.38(2)
Fractional Positions					
Ion (Wyckoff Position)	Gd (4c)	x	0.5199(3)	0.5191(3)	0.5190(3)
		y	0.5793(2)	0.5774(3)	0.5746(2)
		z	0.25	0.25	0.25
	Mn/Fe (4b)	x	0.5	0.5	0.5
		y	0	0	0
		z	0	0	0
	$O1$ (4c)	x	0.081(2)	0.082(2)	0.089(2)
		y	0.495(2)	0.498(2)	0.473(2)
		z	0.25	0.25	0.25
	$O2$ (8d)	x	0.212(2)	0.212(2)	0.218(2)
		y	0.178(2)	0.178(2)	0.174(2)
		z	0.543(1)	0.544(1)	0.548(1)
Interatomic Distances [Å]					
Mn-O1 dist [Å]			1.91(3)	1.92(3)	1.94(3)
Mn-O2 dist [Å]			2.0(2)	2.0(2)	2.0(2)
Octahedral Angle [Deg]					
O1-Mn-O2 ang [Deg]			88.3(2)	88.7(2)	89.7(2)
O2-Mn-O2 ang [Deg]			90.7(2)	91.0(2)	92.1(2)
Mn-O1-Mn ang [Deg]			153.9(3)	153.6(3)	150.2(3)
Mn-O2-Mn ang [Deg]			149.2(2)	149.0(2)	148.0(2)

Source: Authors.

Results of the Rietveld refinement for the $GdMn_{1-x}Fe_xO_3$ samples confirm that, as expected, Fe^{3+} cations occupied the same atomic positions of the Mn^{3+} ions. Figure 2 shows the graphic results of refinement for the three ($x=0.0, 0.1, 0.2$) compositions and Table 1 presents the numerical results of Rietveld refinement.

Influence of the Fe^{3+} substitution in the Mn^{3+} positions is slightly visible on the values of lattice parameters for each material, where it can be observed that with respect to the $GdMnO_3$ in the configurations with $x = 0.1$ and $x = 0.2$, for each 0.1 of substitution, the lattice parameter a grows 0.03% and c grows 0.3%, while the parameter b decreases in 0.5%. As a result of the changes in the cell parameters, the unit cell volume also decreases in 0.1% for each 0.1 of substitution. The most significant changes observed in the structure occur in the positions of the oxygen ions, generating distortions and rotations of the MnO_6 octahedra. These effects are not as marked for the configuration with $x=0.1$ as they are for the configuration with $x=0.2$. In table 1 it can be perceived that the distance between the Mn^{3+} (Fe^{3+}) and O^{2-} ions and the molecular

angles formed between these ions, show changes that are more marked for $x=0.2$ than for $x=0.1$.

In table 1, the decimal number in parentheses denotes the value in which the uncertainty is estimated. Values without parentheses remained fixed during refinement. With respect to the dependence of the crystallographic parameters with the inclusion of Fe^{3+} in the Mn^{3+} sites, it is notable that while the Wyckoff x positions of the Gd increase subtly with the increase in Fe concentration, the y positions decrease. In the same way, the x positions of oxygen O1 and z of oxygen O2 are increased. As a result, the average interatomic distance between the Mn cations and the O1 oxygens, which are located along the vertical line of the MnO_6 octahedra, is increased, as shown in Figure 3. Another parameter that grows slightly is the angle between Oxygen in the octahedra, i.e., O1-Mn-O2 and O2-Mn-O2. These changes suggest that the increase in Fe concentration causes a small expansion of the MnO_6 octahedrons in the structure, which produces the elongation of the crystallographic axes a and c , while the b axis shrinks slightly. Figure 3a exemplifies the perovskite structure $GdMn_{1-x}Fe_xO_3$ within the spatial

group $Pbnm$ (No. 62), while figures 3b and 3c exhibit the pseudocubic perovskite, considering the octahedral distortions within the Glazer representation $a^-a^+c^+$, which denote in phase tilt around the $[100]$ direction and out of phase tilt around the $[001]$ direction of the aristotype [19]. The pseudocubic cell is one that represents the expected cell for a simple perovskite within the complex perovskite. Using VESTA software [20], interatomic distances and tilt angles of pseudocubic representation were calculated with the results reported in table 2. Figures 3b and 3c clearly show the rotations and inclinations of the MnO_6 octahedra in planes bc and ab , respectively. As observed in table 2, the pseudocubic cell parameters present systematical changes with the increase of Fe^{3+} concentration in the material. It is particularly interesting to see that while the pseudo-plane $a'b'$ contracts with the increase in the concentration of Fe^{3+} , the pseudo-axis c' increases. Likewise, the value of

the inclination angles increases, both in phase and out of phase.

From the magnetic point of view, the literature indicates that the Gadolinium manganite not substituted GdMnO_3 evidence type-A antiferromagnetism [7]. Likewise, in the literature there are reports of three phase transitions for this material. The first takes place near $T=23$ K and is related to a transition to type A antiferromagnetism. The second is associated with the spin polarization in Mn^{3+} ions and occurs close to $T=14$ K. A third transition in $T=5$ K is reported to be due to the spin polarization in the Gd^{3+} cations [21]. In Figure 4 the magnetic susceptibility curves as a function of the temperature obtained for all concentrations x are presented in the same graphical scale.

Table 2. Pseudocubic cell parameters and tilt angles in the $a^-a^+c^+$ Glazer representation

Compound	GdMnO_3	$\text{GdMn}_{0.9}\text{Fe}_{0.1}\text{O}_3$	$\text{GdMn}_{0.8}\text{Fe}_{0.2}\text{O}_3$
a', b'	3.94654(7)	3.93739(7)	3.92691(8)
c'	3.72162(9)	3.73439(9)	3.74758(11)
α', β'	90.0000(0)	90.0000(0)	90.0000(0)
γ'	84.6984(18)	84.9713(18)	85.292(2)
Tilt angle (α^-)	16.6875(0)	16.8224(0)	17.6340(3)
Tilt angle (c^+)	13.0696(4)	13.2212(4)	14.9192(5)

Source: Authors.

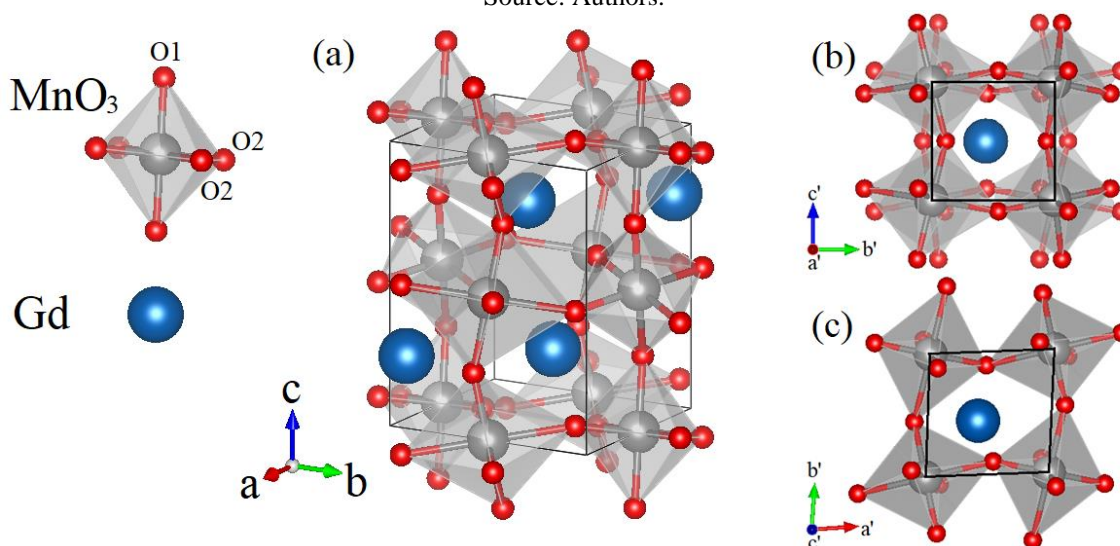


Figure 3. Schematic representation for the structure of $\text{GdMn}_{1-x}\text{Fe}_x\text{O}_3$, constructed by considering the $Pbnm$ space group (# 62), where (a) represents the complex perovskite structure, (b) illustrates the pseudocubic representation ($a^-a^+c^+$) in direction of the a' axis, with out-of-phase rotations of the MnO_6 octahedra, and (c) is the pseudocubic representation ($a^-a^+c^+$) in direction of the c' axis, with in-phase rotations of MnO_6 octahedra. Source: Authors

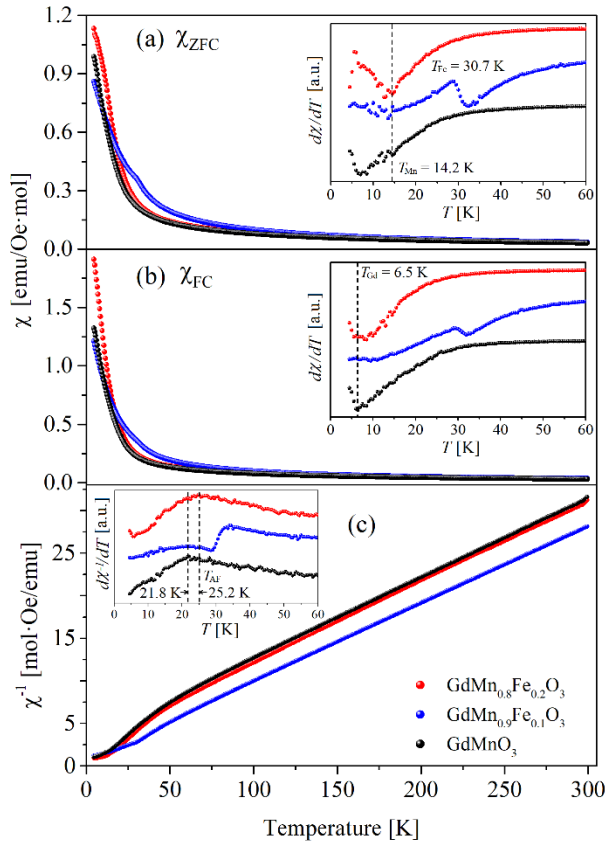


Figure 4. Magnetic behavior of the $\text{GdMn}_{1-x}\text{Fe}_x\text{O}_3$ compounds in the temperature range from 4 K to 300 K. (a) ZFC susceptibility as a function of temperature. (b) FC susceptibility as a function of temperature. (c) Inverse of susceptibility as a function of temperature. The derivative with respect to the temperature is shown on the insets of each figure, in these curves is observed the temperatures of the different magnetic ordering.

Source: Authors.

Figures 4a and 4b represent the Zero Field Cooling (ZFC) and Field Cooled (FC) recipes followed in the susceptibility measure procedure. In the ZFC recipe, the system is frozen in the absence of an applied magnetic field [22]. Then, the field is applied, and the magnetic response is measured as the temperature is increased. Subsequently, it is cooled again while measuring the magnetic susceptibility, but this time in the presence of an external magnetic field, in the well-known FC procedure. The insets of figures 4a and 4b exemplify the temperature derivative of susceptibility, where two phase transitions are evident close to the reported temperatures for the magnetic ordering corresponding to the Mn^{3+} and Gd^{3+} spin contributions. Additionally, for a temperature value around 30.7 K, an anomaly is noticed only for the material corresponding to $x=0.1$. This jump in $d\chi/dT$ could be related with the occurrence of ferrimagnetic

ordering due to the imbalance created by the partial inclusion of Fe^{3+} in the structure. Figure 4c represents the behavior of the inverse of magnetic susceptibility as a function of the temperature, where is clearly observed that above 40 K the material adopts a paramagnetic behavior. The inset shows the derivative of the susceptibility curves. In these graphs the transition between the paramagnetic and antiferromagnetic states can be observed for all the curves (~ 21.8 K - 25.2 K), as well as the anomaly observed at 30.7 K for $x=0.1$.

A schematic model to explain why the transition to 30.7 K is only observed for $x = 0.1$ is represented in figure 5.

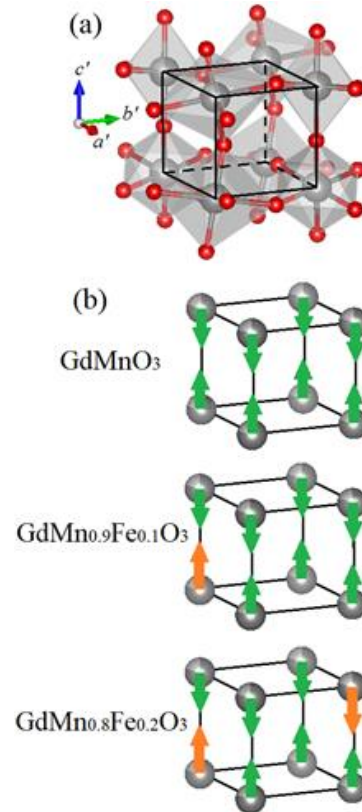


Figure 5. Schematic model of Mn^{3+} and Fe^{3+} arrangement in the pseudocubic cell. Green arrows represent the magnetic moment of Mn^{3+} ions and orange arrows represent the magnetic moment of Fe^{3+} ions.

Source: Authors.

The left side (figure 5a) shows the pseudocubic structure mentioned above, and the right side (figure 5b) presents a possible arrangement of the Mn^{3+} and Fe^{3+} ions in this structure for $x=0.0$, 0.1 and 0.2 . A substitution $x=0.1$ means that one in ten ions in the corners of this structure corresponds to a Fe^{3+} ion, whereby, it is very likely that in this cell, only one corner will be occupied by one Fe^{3+} ion, thus generating an unbalanced cell, since the

Table 3. Magnetic parameters obtained from the Curie-Weiss fitting, performed on the susceptibility curve, which was calculated from the susceptibility curves of figure 4. The value in parentheses denotes uncertainty

Material	C [emu.K/mol.Oe]	θ_p [K]	μ_{eff} [μ_B]
GdMnO_3	10.55(2)	-33.4(4)	9.18(4)
$\text{GdMn}_{0.9}\text{Fe}_{0.1}\text{O}_3$	10.88(8)	-7.8(2)	9.32(4)
$\text{GdMn}_{0.8}\text{Fe}_{0.2}\text{O}_3$	10.47(2)	-27.2(3)	9.14(4)

Source: Authors.

effective magnetic moment of Fe^{3+} is larger than that of Mn^{3+} . On the other hand, in the case of $x = 0.2$, it is more likely that two corners contain Fe^{3+} ions (two out of ten ions), therefore their magnetic moments can be antiparallel, which results in an antiferromagnetic behavior similar to the material without substitution (with $x = 0.0$).

It is possible to perform a similar analysis thinking that the distorted perovskite structure, which was presented in figure 3a, contain four ions of Mn^{3+} (Fe^{3+}) in its unit cell, i.e., eight in two consecutive cells. Therefore, it could be said that, for $x = 0.1$, there is only one Fe^{3+} ion in most consecutive cell pairs, which gives rise to an imbalance in the magnetic moment. Meanwhile, for $x = 0.2$, in most of the unit cells there is an Fe^{3+} ion, and thus, a magnetic moment of a cell would be canceled with the opposite moment of the neighboring cell.

Results of the Curie-Weiss adjustment performed on the magnetic susceptibility are showed in table 3. The effective magnetic moment calculated from the experimental data for GdMnO_3 ($x=0.0$) was $\mu_{eff} = 9.18 \mu_B$, which agrees with the value reported by other authors for this material ($9.2 \mu_B$) [21].

As can be seen in table 3, the effective magnetic moment for the cases $x = 0.0$ and $x = 0.2$ is very similar, constituting a result consistent with the similarity presented by the magnetic susceptibility curves presented in figure 4 for these two concentrations of Fe^{3+} .

On the other hand, in the case of $x=0.1$, where the magnetic susceptibility curve of figure 4 shows significant changes with respect to the cases mentioned above, a greater effective magnetic moment is obtained, which reinforces the hypothesis of occurrence of an imbalance in the antiferromagnetic arrangement within the unit cell, which is generated by the distribution of Fe^{3+} in the crystal structure of $\text{GdMn}_{0.9}\text{Fe}_{0.1}\text{O}_3$, giving rise to a ferrimagnetic type response, as schematized in figure 5.

4. Conclusions

Compounds $\text{GdMn}_{1-x}\text{Fe}_x\text{O}_3$ ($x=0, 0.1, 0.2$) were obtained by the conventional solid-state reaction method, observing that the expected phase is majority after thermal treatments at temperature values above 1000°C , obtaining phases with high purity and crystallinity at sintering temperatures of 1200°C . Rietveld refinement showed that the materials crystallizes in an orthorhombic structure (Pbnm No. 62 space group) for three studied concentrations of Fe^{3+} substituted in the Mn^{3+} crystallographic sites, with slightly variation in the lattice parameters for each value of x and more notable influence in the positions of the oxygen ions, i.e., in the octahedral tilting and rotation. Analysis of the magnetic response in curves of magnetic susceptibility as a function of temperature revealed that this material behaves as a paramagnetic at high temperatures, evidencing phase transitions to the antiferromagnetic state close 25 K for all x concentrations. It is assumed that the inclusion of Fe^{3+} in the Mn^{3+} sites of the crystal structure, lead to a ferrimagnetic state for $x=0.1$, which can be seen at 30.7 K, as a result of the inclusion of an imbalance in the magnetic moment into the unit cell. This result suggests that it is possible to tune the ferrimagnetic character of the material by controlling the magnetic moment in the unit cell, by manipulating the concentration of Fe^{3+} in the structural positions of Mn^{3+} .

Acknowledgments

This work was partially financed by Ministerio de Ciencia y Tecnología – Minciencias, on the project FP80740-243-2019. One of us (J.A. Cardona Vasquez) received support by Minciencias, on the scholarship program for national doctorates.

References

- [1] K.A. Müller, T.W. Kool, *Properties of Perovskites and other oxides*. Singapore: World Scientific Publishing Co. Pte. Ltd., 2010.

- [2] C.E. Deluque, A.V. Gil, J.I. Villa, D.A. Landínez Téllez, J. Roa-Rojas, “Half-metallic electronic feature and thermophysical properties of the $\text{Ba}_2\text{CoMoO}_6$ perovskite-like cobalt molybdate,” *Revista UIS Ingenierías*, vol. 19, no. 1, pp. 213-224, 2020, doi: 10.18273/revuin.v18n4-2020020
- [3] F. Dogan, H. Lin, M. Guilloux, O. Peña, “Focus on properties and applications of perovskites,” *Sci. Technol. Adv. Mater.* vol. 16, no. 2, pp. 020301, 2015, doi: 10.1088 / 1468-6996 / 16/2/020301
- [4] A. Urushibara, Y. Moritomo, T. Arima, A. Asamitsu, G. Kido, Y. Tokura, “Insulator-metal transition and giant magnetoresistance in $\text{La}_{1-x}\text{Sr}_x\text{MnO}_3$,” *Phys. Rev. B*, vol. 51, no. 20, pp. 14103-14109, 1995, doi: 10.1103/PhysRevB.51.14103.
- [5] N.A. Spaldin, *Magnetic Materials Fundamentals and Applications*. New York, NY, USA: Cambridge University Press, 2011.
- [6] R.D. Johnson, D.D. Khalyavin, P. Manuel, L. Zhang, K. Yamaura, A.A. Belik, “Magnetic structures of the rare-earth quadruple perovskite manganites $\text{RMn}_7\text{O}_{12}$,” *Phys. Rev. B*, vol. 98, no. 10, pp. 104423-1 - 104423-10, 2018, doi: 10.1103/PhysRevB.98.104423
- [7] H. Liu, X. Yang, “A brief review on perovskite multiferroics,” *Ferroelectrics*, vol. 507, no. 1, pp. 69-85, 2017, doi: 0.1080/00150193.2017.1283171
- [8] S. Dong, R. Yu, S. Yunoki, J.M. Liu, E. Dagotto, “Double-exchange model study of multiferroic RMnO_3 perovskites,” *Eur. Phys. J. B*, vol. 71, no. 3, pp. 339-344, 2009, doi: 10.1140/epjb/e2009-00225-1
- [9] J. Dho, W.S. Kim, E.O. Chi, N.H. Hur, S.H. Park, H.C. Ri, “Colossal magnetoresistance in perovskite manganite induced by localized moment of rare earth ion,” *Sol. Stat. Commun.*, vol. 125, no. 3-4, pp. 143-147, 2003, doi: 10.1016/S0038-1098(02)00775-5
- [10] P.P. Rout, S.K. Pradhan, S.K. Das, B.K. Roul, “Room temperature ferroelectricity in multiferroic HoMnO_3 ceramics,” *Physica B*, vol. 407, no. 12, pp. 2072-2077, 2012, doi: 10.1016/j.physb.2012.02.007
- [11] S. Dong, R. Yu, S. Yunoki, J.M. Liu, E. Dagotto, “Double-exchange model study of multiferroic RMnO_3 perovskites,” *Eur. Phys. J. B*, vol. 71, no. 3, pp. 339, 2009, doi: 10.1140/epjb/e2009-00225-1
- [12] D.I. Khomskii, “Coupled Electricity and magnetism in Solids,” *Multiferroic Materials: Properties, Techniques and Applications*, Ed. by J. Wang, CRC. New York, NY, USA: Press Taylor & Francis, 2017, pp. 54-65.
- [13] J.A. Cardona, D. A. Landínez Téllez, J. Roa-Rojas, “Physical properties of the new multiferroic perovskite-like material $\text{HoMn}_{1-x}\text{Fe}_x\text{O}_3$,” *Physica B*, vol. 455, no. 24, pp. 39-43, 2014, doi: 10.1016/j.physb.2014.07.041
- [14] J.A Cardona, D. A. Landínez Téllez, C. A. Collazos, J. Roa-Rojas, “Structural and magnetic characterization of the new $\text{GdMn}_{1-x}\text{Fe}_x\text{O}_3$ perovskite material,” *J. Phys.: Confer. Ser.*, vol. 687, no. 1, pp. 012087-1 – 012087-4, 2015, doi: 10.1088/1742-6596/687/1/012087
- [15] A. Pal, P. Murugavel, “Investigations on the effect of magnetic ordering on dielectric relaxation in polycrystalline $\text{GdMn}_{1-x}\text{Fe}_x\text{O}_3$,” *Physica B*, vol. 555, no. 3, pp. 99-105, 2019, doi: 10.1016/j.physb.2018.11.057
- [16] C.A. Triana, D. A. Landínez Téllez, J. Roa-Rojas, “General study on the crystal, electronic and band structures, the morphological characterization, and the magnetic properties of the $\text{Sr}_2\text{DyRuO}_6$ complex perovskite,” *Mater. Character.*, vol. 99, no. 1, pp. 128–141, 2015, doi: 10.1016/j.matchar.2014.11.021
- [17] A.C. Larson, R.B. Von, “General Structure Analysis System (GSAS)” USA: Los Alamos National Laboratory Report LAUR, pp. 86, 2004.
- [18] B.H. Toby, “EXPGUI, a graphical user interface for GSAS,” *J. Appl. Cryst.*, vol. 34, no. 2, pp. 210-213, 2001, doi: 10.1107/S0021889801002242
- [19] A.M. Glazer, “The classification of tilted octahedra in perovskites,” *Acta Cryst. B*, vol. 28, pp. 3384-3392, 1972, doi: 10.1107/S0567740872007976
- [20] K. Momma y F. Izumi, “VESTA 3 for three-dimensional visualization of crystal, volumetric and morphology data,” *J. Appl. Cryst.*, vol. 44, pp. 1272-1276, 2011, doi: 10.1107/S0021889811038970

[21] W.S. Ferreira, J.A. Moreira, A. Almeida, M.R. Chaves, J.P. Araújo, J.B. Oliveira, J.M. Machado, M.A. Sá, T.M. Mendonça, P. Simeão, J. Kreisel, J.L. Ribeiro, L.G. Vieira, P.B. Tavares, S. Mendonça, “Spin-phonon coupling and magnetoelectric properties: EuMnO_3 versus GdMnO_3 ,” *Phys. Rev. B*, vol. 79, no. 5, pp. 054303-1 – 054303-6, 2009, doi: 10.1103/PhysRevB.79.054303

[22] J.A. Cuervo, D.M. Aljure, R. Cardona, J.A. Rodríguez, D.A. Landínez Téllez, J. Roa-Rojas, “Structure, ferromagnetic, dielectric and electronic features of the $\text{LaBiFe}_2\text{O}_6$ material,” *J. Low Temp. Phys.*, vol. 186, no. 5-6, pp. 295–315, 2017, doi: 10.1007 / s10909-016-1714-6